



Wave dispersion and attenuation in fresh mortar: theoretical predictions vs. experimental results

D.G. Aggelis^{a,b}, D. Polyzos^{a,b}, T.P. Philippidis^{a,b,*}

^a*Department of Mechanical Engineering and Aeronautics, University of Patras, P.O. Box 1401,
Panepistimioupolis, Rion 26504, Greece*

^b*Institute of Chemical Engineering and High Temperature Chemical Processes,
(FORTH/ICE-HT) Patras 26500, Greece*

Received 28 May 2004; received in revised form 18 November 2004; accepted 21 November 2004

Abstract

In the present paper, the dispersive and attenuative behavior of fresh cementitious material is examined through a series of ultrasonic, through-transmission measurements. The sand size and content dominate attenuation behavior, while the effect of entrapped air bubbles is mostly obvious at lower frequencies elevating phase velocity to values much higher than that of water. Theoretical investigation seems to explain the observed dispersion and attenuation mainly through two scattering interactions: sand embedded in paste and air bubbles in mortar. The predictions made by scattering theory follow closely the experimental data. The possibility of material characterization is discussed.

© 2005 Elsevier Ltd. All rights reserved.

Keywords: Fresh concrete; Ultrasonic wave dispersion; Attenuation; Water-to-cement ratio

1. Introduction

Concrete is the most widely used construction material worldwide. Its behavior is strongly time-dependent since, just after mixing, it starts as a liquid suspension of

*Corresponding author. Department of Mechanical Engineering and Aeronautics, University of Patras, P.O. Box 1401, Panepistimioupolis, Rion 26504, Greece. Tel./fax: +30 2610 997235.

E-mail address: philippidis@mech.upatras.gr (T.P. Philippidis).

particles, i.e. cement, sand grains, coarse aggregates and air bubbles, suspended in water, while the hydration reaction transforms it into a porous solid medium with considerable load-bearing capacity. The initial mix proportions and especially the water-to-cement ratio by mass, w/c , is a key factor for its final strength and durability (Abrams, 1918; Neville, 1995) mainly due to the porosity resulting from excessive water. Although for any particular application, a certain mix can be designed, in many cases, this is not the material actually placed in the site. This could be due to incorrect weighting (Neville, 1995; Mubarak et al., 2001) or even deliberate addition of water, since operators unfamiliar with cement chemistry are often tempted to increase w/c in order to improve workability and slump (Neville, 1995; Bescher et al., 2004). By ensuring that all standard procedures are followed and that concrete is batched according to the selected mixture proportions, the possibilities of inadequate service life are essentially reduced (Mather, 1976). Therefore, the importance of assessing the quality of concrete while it is still fresh has been highlighted (Mather, 1976; Popovics and Popovics, 1998).

Many different approaches have been followed toward fresh concrete w/c determination. Although this paper deals with stress wave propagation, the interested reader is directed to the following sources for initial information concerning other techniques (Malhotra and Carino, 1998; Head et al., 1983).

As for wave propagation, several studies concerning examination of fresh cementitious material have been reported, aiming, not exclusively at the determination of w/c (Popovics and Popovics, 1998), but also at the general assessment of concrete quality, with the set point determination (i.e. the time when concrete obtains a certain level of desirable rigidity, according to the given application) being of certain importance for a number of cases (Labouret et al., 1998; Ozturk et al., 1999; Subramanian et al., 2000; Rapoport et al., 2000; Garnier et al., 1995; Keating et al., 1989; D'Angelo et al., 1995; Sayers and Dahlin, 1993; Valic, 2000; Grosse and Reinhardt, 2001; Chotard et al., 2001).

Qualitatively, it has been shown that material with low w/c exhibits higher pulse velocity as well as higher amplitude measured through transmission (Grosse and Reinhardt, 1994; Reinhardt et al., 2000; Boumiz et al., 1996; Casson and Domone, 1982; Boutin and Arnaud, 1995; Arnaud and Thinet, 2003; Ye et al., 2003) or reflection configurations (Valic, 2000; Chotard et al., 2001; Akkaya et al., 2003).

However, the reliable estimation of w/c has not yet been reached, neither has the propagation behavior been explicitly explained. The severe attenuation has been attributed to the strongly inhomogeneous nature of the material, the role of entrapped air bubbles, during mixing, being pointed out (Popovics and Popovics, 1998; Sayers and Dahlin, 1993; Boutin and Arnaud, 1995; Arnaud and Thinet, 2003; Herb et al., 1999), despite its relatively low volume content ($< 10\%$).

During the present work, an experimental series of ultrasonic measurements in fresh mortar was conducted. The study concerned a wide range of frequencies, namely between 20 kHz and 1 MHz, since the influence of the individual phases present in the material, due to different characteristic size and physical properties, are expected to be pronounced at different frequencies. Initial results (Aggelis and Philippidis, 2004) highlighted the dependence of pulse velocity and high-frequency

attenuation on the sand content, while the connection of w/c to these wave parameters was not obvious.

In this work, results from longitudinal phase velocity measurements are presented, conducted for frequencies up to 1 MHz. A theoretical investigation of the mechanisms responsible for the obtained experimental phase velocity dispersion and attenuation is undertaken through multiple scattering theory. To this end, the simple multiple scattering theory proposed by [Waterman and Truell \(1961\)](#) is employed. According to this theory, the wave dispersion and attenuation taking place in a particulate composite medium can be obtained in terms of the particle concentration and the forward as well as the backward far field scattering amplitudes. These in turn are derived from the solution of the single particle wave scattering problem dealing with the interaction of a longitudinal plane wave of given frequency with an inclusion surrounded by the matrix medium. Due to the experimentally observed dependence of mortar high-frequency attenuation (>300 kHz) on the sand grain size as well as the severe attenuation of cement paste at low frequencies (<300 kHz) in the present work, theoretical predictions were made by considering the cementitious material first as a suspension of spherical sand particles embedded in cement paste and next as a suspension of air bubbles in fresh mortar. Both forward and backward single scattering parameters required in [Waterman and Truell's](#) dispersion and attenuation expressions are evaluated analytically by means of the [Ying and Truell \(1956\)](#) solution of the corresponding single scattering problems. The Ying and Truell formulation is employed, due to its simplicity and generality of use, since with proper modification of the constituents' physical properties, any case of scattering interaction can be addressed (e.g. elastic–elastic, elastic–liquid) ([Pao and Mow, 1963](#); [Challis et al., 1998](#)). The implementation of the scattering amplitudes obtained to the dispersion relation of [Waterman and Truell \(1961\)](#) provides phase velocity and attenuation predictions quite close to the experimental results.

This paper aims to improve the understanding of wave propagation in fresh cementitious material, examining the possibility of enhancing composition characterization capabilities.

2. Experimental procedure and measurements

The experimental setup, described in detail in [Aggelis and Philippidis \(2004\)](#), consists of a Physical Acoustics Corporation (PAC) waveform generator WaveGen 1410, two broadband transducers Panametrics V413 of 500 kHz center frequency, PAC preamplifier 1220A and a PAC Mistras 2001 acoustic emission data acquisition system. The rectangular sensors are mounted in plexi-glass plates facing each other at a distance of 10.6 mm, while a U-shaped rubber plate is placed in between defining the volume to be occupied by the specimen; see [Fig. 1](#).

The waveforms selected as electric input to the transducer are of the shape seen in [Fig. 2\(a\)](#). This sinusoidal wave in sinusoidal envelope introduces a relatively narrowband excitation to the sensor, as can be seen in [Fig. 2\(b\)](#), where the Fourier

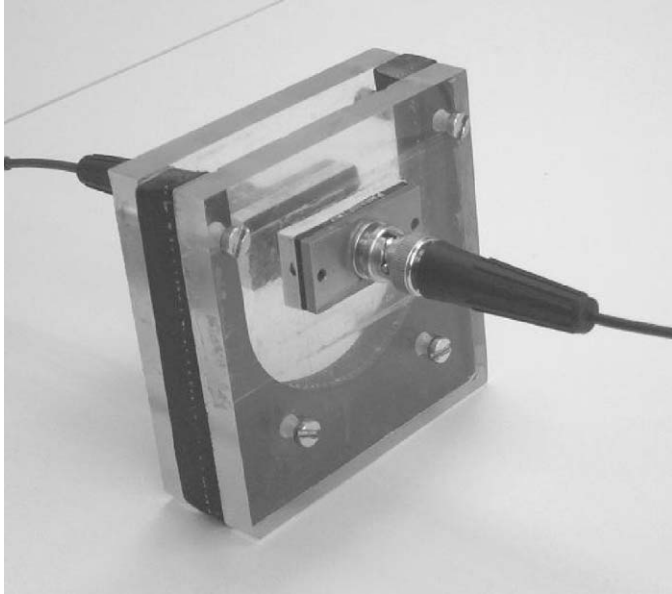


Fig. 1. Fresh mortar container and ultrasonic sensors.

transform of the above signal is depicted. Several similar tone-burst signals are used with central frequencies from 20 kHz up to about 1 MHz at certain intervals. Due to severe attenuation, in most cases, reliable signals were acquired up to 800 kHz. The use of broadband excitation has also been adopted through the introduction of sine-sweep pulses, as seen in Fig. 2(c). This way the electric signal exhibits approximately constant magnitude throughout the first MHz as seen in Fig. 2(d) and depending of course on the sensor's response, a wide range of frequencies enter the material.

Mortar containing various sand contents by volume, s , from 0%, which is simply cement paste, up to even 47.5% and different w/c in a range widely used in practice was produced and tested. The ingredients (cement II 32.5, limestone sand and water) were mixed and stirred for 5 min. Then, the material was poured between the sensors and compacted by means of a stick, which resulted in the release of visible air bubbles on the surface.

2.1. Attenuation measurements

The poorly understood nature of wave propagation in such systems complicates greatly the task of quantifying the contributions of different mechanisms (absorption, visco-inertial losses, thermal dissipation losses and scattering) to the total attenuation.

In the present study, total attenuation was calculated using the spectra of the sine-sweep pulses through the examination material. These spectra were normalized with a point by point division with the reference spectrum, which in this case comes from

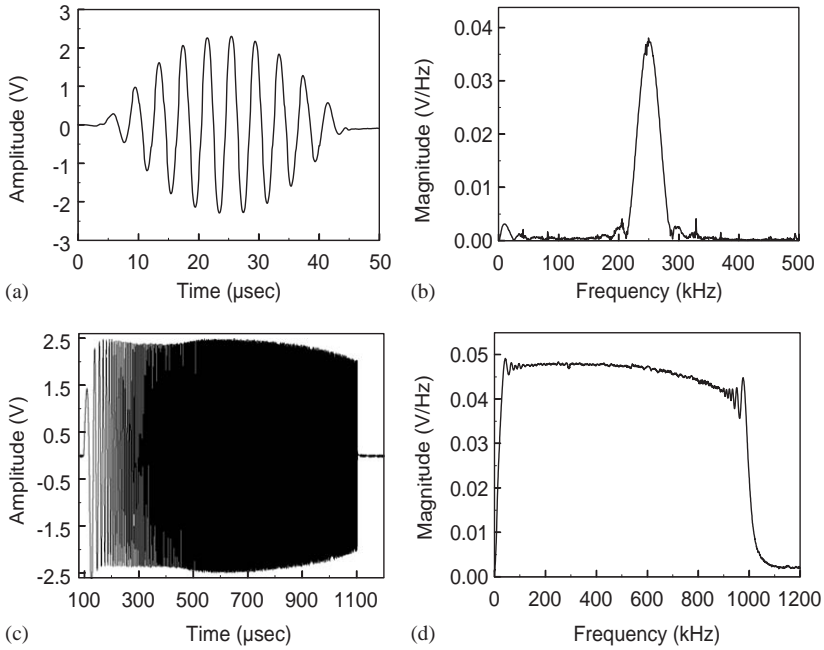


Fig. 2. Input electric signal of 10 cycles at 250 kHz in sinusoidal envelope in time domain (a) and in frequency domain (b), 10 kHz–1 MHz sine-sweep electric signal in time domain (c) and in frequency domain (d).

a water specimen

$$Att(f) = -\frac{20}{x} \log\left(\frac{A(f)}{A_w(f)}\right). \tag{1}$$

$Att(f)$ stands for the attenuation with respect to frequency, x is the distance between the sensors (10.6 mm) and $A(f)$ and $A_w(f)$ are FFT magnitudes of signals from the spectra of the mortar specimen and water, respectively. Water is considered ideal in this case; therefore, its amplitude resembles the amplitude of the pulse entering the specimen. The sampling rate of 10 MHz is adequate for the digitization of even the last part of the sine-sweep signal containing frequencies up to 1 MHz. Therefore, the digitized waveform can be reliably used for determination of frequency content of the wave propagating through the material and the attenuation of each frequency. Geometric attenuation, i.e. wavefront spreading, always has the same effect since all specimens used for attenuation measurements are of the same size. An example of mortar with $w/c = 0.525$ attenuation curves is given in Fig. 3 for different sand content. It is seen that the sand content has a severe impact on measured attenuation at frequencies above 300 kHz, while it also affects strongly low-frequency attenuation.

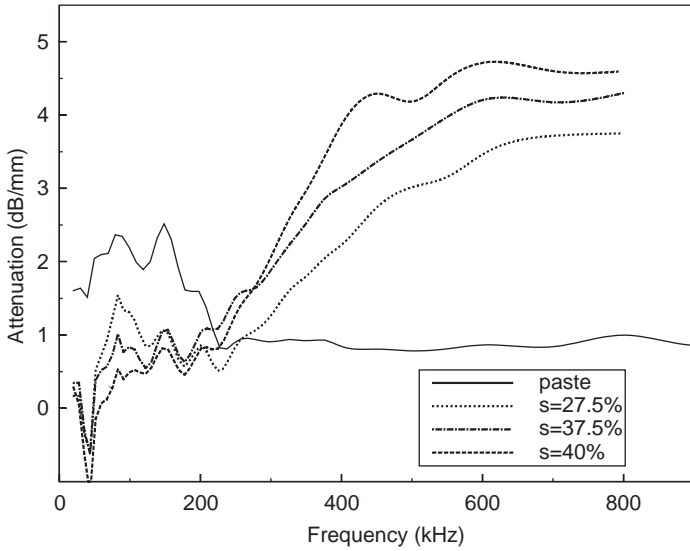


Fig. 3. Effect of sand content on frequency-dependent attenuation in mortar with $w/c = 0.525$. Experimental results.

2.2. Phase velocity measurements

The pulse used, as mentioned above, is of the form of Fig. 2(a). While traveling in a non-dispersive medium, this envelope will experience no shape distortion. For dispersive wave propagation, however, the individual peaks within the wave packet will move relatively to the centroid as the wave propagates through the medium. Pulse velocity is generally defined as the specimen thickness divided by the transit time t ; see Fig. 4(a). This transit time is dependent usually on an amplitude threshold. Phase velocity, on the other hand, is determined from the position of reference “phase” points of the waveforms on signals recorded using different wavepaths. Specifically for any composition to be tested, two specimens were prepared with thickness 10.25 and 18.55 mm. These specimens were interrogated with 10 cycle tone bursts of 30 different central frequencies from 20 kHz to 1 MHz. Phase velocities were calculated as the ratio of the thickness difference of the two specimens, namely 8.3 mm to the transit time of the phase points, δt (Kinra et al., 1980). As such, the 4th to 7th peaks of each waveform were considered; see Fig. 4, where the phase points on two waveforms are depicted. These waveforms are of central frequency 400 kHz and were collected after propagation through 10.25 mm (Fig. 4(a)) and 18.55 mm (Fig. 4(b)) in the same composition specimens. Specifically, for further accuracy, the time differences between the corresponding peaks of each waveform were averaged to yield the time delay used in phase velocity measurements. Typical phase velocity vs. frequency results are depicted in Fig. 5

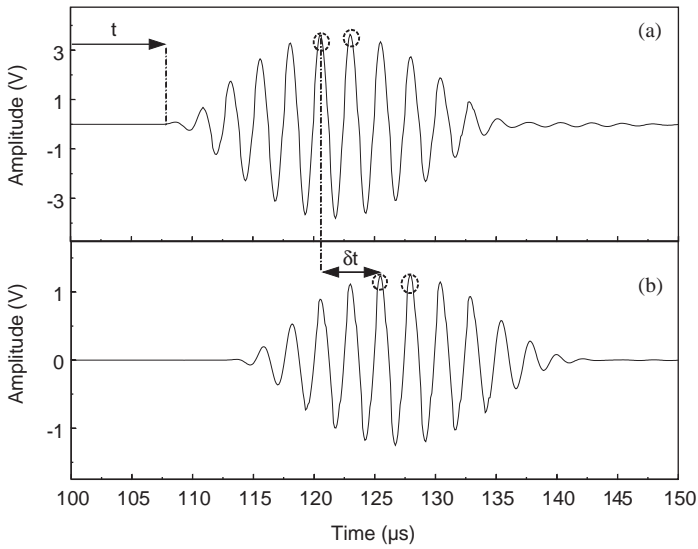


Fig. 4. Four hundred kilohertz central frequency signal after propagation through 10.25 mm (a) and 18.55 mm (b) of cementitious material.

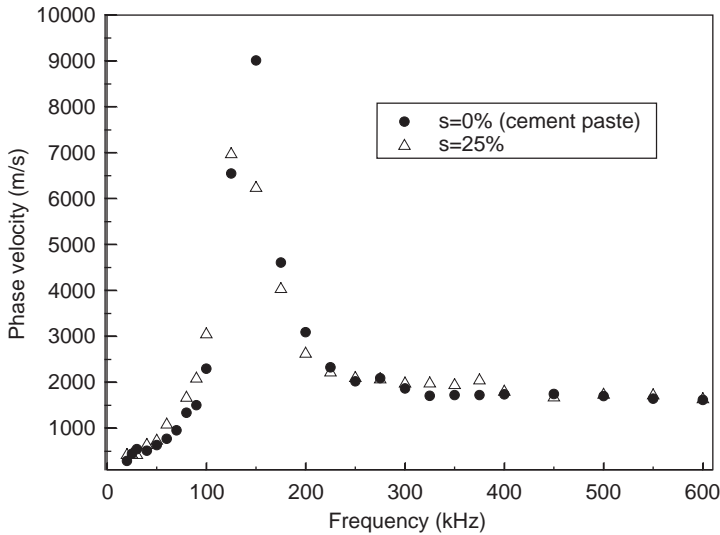


Fig. 5. Effect of sand content on dispersion curves of mortar with $w/c = 0.55$. Experimental results.

for cement paste and mortar with $s = 25\%$. It is seen that at around 150 kHz, the phase velocities increase to values approaching 10000 m/s for these materials, behavior typically attributed to air bubbles when suspended in liquid (Sayers and Dahlin, 1993; Temkin, 2000).

3. Theoretical modeling

A number of indications lead to the conclusion that lossless redirective scattering, henceforth denoted simply scattering, is the dominant mechanism in wave propagation in the material at hand. Such indications, as has been stated and will be extensively studied below, are the strong influence of sand content on high-frequency attenuation, as well as the influence of sand grain size.

In order to investigate the influence of sand particles on ultrasonic parameters, the simple multiple scattering theory of [Waterman and Truell \(1961\)](#) is employed. It is well known that a pulse propagating in a particulate composite material undergoes both dispersion and attenuation due to its interaction with the embedded particles. According to the [Waterman and Truell multiple scattering model](#), this wave dispersion and attenuation is represented via a frequency-dependent complex wavenumber, $k(\omega)$, expressed in terms of the particle concentration and the forward as well as the backward far-field scattering amplitudes. The latter are taken from the solution of the single particle wave scattering problem where a plane wave of given frequency impinges upon a particle suspended in the matrix medium, i.e.

$$\left(\frac{k(\omega)}{k_c}\right)^2 = 1 + \frac{3\varphi}{k_c^2 R^3} f(0) + \frac{9\varphi^2}{4k_c^4 R^6} [f^2(0) - f^2(\pi)], \quad (2)$$

where k_c is the real wavenumber of the matrix material, φ the volume fraction of the inclusion, R the particle radius when spherical particles are considered and $f(0)$ and $f(\pi)$ are the complex single scattering forward and backward scattering amplitudes, respectively.

Eq. (2) refers to the case of one population of spherical inclusions present in the composite medium. In case different size populations of inclusions are present, the scattering amplitudes derived from Eq. (2) after processing each problem separately are applied in the dispersion relation weighted according to the volume fraction of the corresponding phases as follows, for the general case of i different phases ([McClements, 2000](#)):

$$\left(\frac{k}{k_c}\right)^2 = 1 + \frac{3}{k_c^2} \sum_i \frac{\varphi_i f_i(0)}{R_i^3} + \frac{9}{4k_c^4} \sum_i \frac{\varphi_i^2}{R_i^6} [f_i^2(0) - f_i^2(\pi)]. \quad (3)$$

Frequency-dependent phase velocity, $c(\omega)$ and attenuation coefficient, $a(\omega)$, are calculated from

$$k(\omega) = \frac{\omega}{c(\omega)} + i\alpha(\omega), \quad (4)$$

where ω is the angular frequency.

The single scattering parameters required in Eqs. (2) and (3) are evaluated here by means of the corresponding analytical expressions provided by [Ying and Truell \(1956\)](#). Using their formulation, the problem of a longitudinal plane wave impinging on a spherical obstacle is dealt with, taking into account the continuity of displacements and stresses on the scatterer–matrix interface. It is noted that the

original Ying and Truell formulation concerns scattering from an elastic inclusion embedded in an elastic matrix. In case the modeling concerns a problem of scattering from particles suspended in liquid, the equations can be derived by a limiting process where the shear modulus of the host medium obtains an infinitely small value ($\mu \rightarrow 0$) (Pao and Mow, 1963; Challis et al., 1998).

Other well-known formulations of the diffraction problem for a compression wave incident on a single scatterer (Epstein and Carhart, 1953; Allegra and Hawley, 1972) contain two additional equations, originating from the continuity of temperature and heat flux. Thermal mechanisms, however, are generally considered dominant for suspensions where the dispersed and continuous phase share approximately the same density (Dukhin and Goetz, 1996; Holmes et al., 1993). In the present case, sand with density of 2650 kg/m^3 suspended in cement paste with density around 1800 kg/m^3 is quite far apart, while the density contrast between air bubbles and the surrounding mortar does not need to be highlighted. Moreover, scattering is the governing effect for large particles (Hipp et al., 1999), i.e. comparable to the wavelength, which is the case for mortar and the frequencies used herein. Anyway, the agreement between experimental results with theoretical ones, obtained by means of the Ying and Truell formulation in this work, shows that it is adequate to describe the propagation behavior of such a suspension at least to a certain extent without the implication of thermal terms. It is also noted that all the above-cited scattering formulations can be considered equivalent in case thermal effects are omitted (Challis et al., 1998).

Therefore, with the knowledge of scattering coefficients, A_n , which are functions of the amplitude of the scattered wave, obtained using the Ying and Truell formulation, the far-field forward and backward scattering amplitudes $f(0)$ and $f(\pi)$ can be calculated through (Challis et al., 1998)

$$\begin{aligned} f(0) &= \frac{1}{ik} \sum_{n=0}^{\infty} (2n+1)A_n, \\ f(\pi) &= \frac{1}{ik} \sum_{n=0}^{\infty} (-1)^n (2n+1)A_n. \end{aligned} \quad (5)$$

In order to explain the obtained experimental results, two multiple scattering problems in terms of relations (2) and (3) have been solved in the present work. The first problem concerns sand particles embedded in a cement paste matrix, while the second one deals with air bubbles suspended in a mortar medium whose homogenized material properties are extracted as explained in the sequel. The configuration of the two problems addressed is schematically depicted in Fig. 6.

3.1. Sand particle influence

For the first case, i.e. scattering on sand, Fig. 6(a) is of interest. Cement paste is considered as the continuous host medium, in which one size, spherical sand particles are suspended. The physical properties of sand (Young's modulus E_s , Poisson ratio ν_s and density ρ_s) are given in Table 1. The radius used (1.4 mm) is a mean value

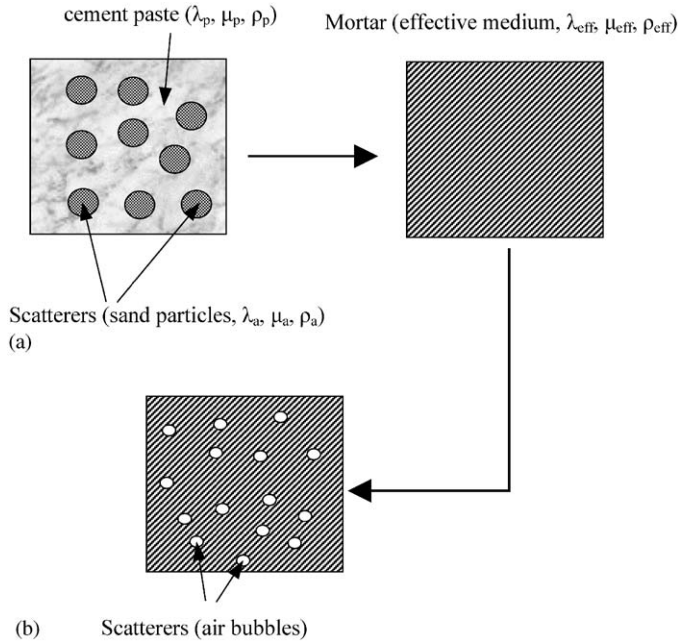


Fig. 6. Model configuration: (a) sand particles in cement paste, (b) air bubbles in mortar.

Table 1
Parameter values applied to scattering model

R_z (mm) (radius)	1.4			
E_z (GPa)	30			
ν_z	0.2			
ρ_z (g/cm ³)	2.69			
			Paste	Mortar
φ_{air1} (%)	.55	R_{air1} (mm)	1.0	1.4
φ_{air2} (%)	.25	R_{air2} (mm)	.88	1.2
φ_{air3} (%)	.45	R_{air3} (mm)	.75	1.1
φ_{air4} (%)	.45	R_{air4} (mm)	.62	1.1
φ_{air5} (%)	.45	R_{air5} (mm)	.50	1
$\varphi_{airtotal}$ (%)	2.15			

since particle sizes range from 1 to 4 mm. On the other hand, material properties of the cement paste matrix are derived as follows.

Density, ρ_m , of cementitious materials containing cement, sand and water can be quite accurately calculated as

$$\rho_m = \frac{c + \alpha + w}{V_c + V_\alpha + V_w} = \frac{c + \alpha + w}{c/\rho_c + \alpha/\rho_\alpha + w/\rho_w} = \frac{w/c + 1 + \alpha/c}{1/\rho_c + \alpha/c\rho_\alpha + w/c\rho_w}, \quad (6)$$

where c , α , w are the masses of cement, sand and water, respectively, V_c , V_α , V_w the corresponding volumes and ρ_c , ρ_α , ρ_w the corresponding densities. In the case of cement paste, the same equation is used setting $\alpha = 0$.

As has been seen in Fig. 5, phase velocity, C_p , of any different mix ends up to the same value of about 1650 m/s at high frequencies regardless of the mix proportions. Therefore, the bulk modulus K for the paste matrix considered is calculated through

$$K = \rho_m C_p^2. \quad (7)$$

Discussion concerning the selection of the adequate value for the equivalent shear modulus, μ , of the host medium will follow in the next section. In this case, however, this selection is of limited importance since values of μ from the order of 0 to 10^8 Pa yield identical attenuation curves. Only when the shear rigidity of the matrix becomes comparable to that of a solid medium (μ approaches 10^9 Pa), the attenuation diminishes significantly, which is hardly the case for cement paste. For the specific results, however, the shear modulus was set equal to 30 MPa.

Implementation of material properties as obtained above to the Ying and Truell model, to yield scattering amplitudes from Eq. (5) and application of the Waterman and Truell dispersion relation, Eq. (2), leads to phase velocity, $c(\omega)$ and attenuation coefficient, $\alpha(\omega)$, predictions from Eqs. (3) and (4).

As stated in Section 2.1, the experimentally measured attenuation was derived from the division of the signal amplitude from the test specimen and reference (water) amplitudes through Eq. (1). In theory, a plane longitudinal wave propagating in x -direction of a medium assumes the form $e^{i(kx - \omega t)}$, where k is complex. Considering different phase velocities and attenuation coefficients for mortar and water, the ratio of their amplitudes expressed in dB is given by

$$\text{Att}(f) = -\frac{20}{x} \log \left| \frac{e^{i((\omega/c(f)) - \alpha(f))x}}{e^{i((\omega/c_w) - \alpha_w)x}} \right|, \quad (8)$$

where $c(f)$ and $\alpha(f)$ are the phase velocity and attenuation coefficient of mortar, obtained by solving the scattering problem and c_w and α_w are the phase velocity and attenuation coefficient of water, respectively. Water is considered non-dispersive with a sound velocity, c_w , of 1500 m/s while its attenuation coefficient was set at a small constant value (5.4/m) to match experimental guiding results, since attenuation of cement paste at high frequencies does not diminish to 0, but reaches a constant value, as seen in Fig. 3. Therefore, it could be said that the applied α_w accounts to some extent for dissipative mechanisms acting in cement paste. This process was followed to make valid comparison of theoretical and experimental attenuation values, since measurements, as stated, employed the water amplitude normalization.

As can be seen in Fig. 7(a), the theoretical curves obtained from scattering on sand particles are appropriate to describe the rise of the experimental ones for frequencies above about 300 kHz. The sand volume fraction seems to dominate high-frequency attenuation since for cement paste, which contains no sand, the attenuation seems

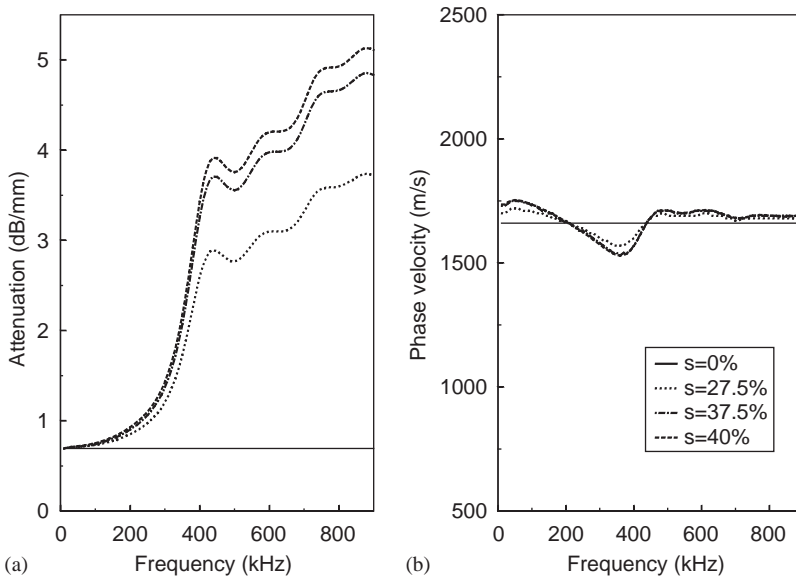


Fig. 7. Effect of sand content on frequency-dependent attenuation (a) and dispersion curves (b) of mortar with $w/c = 0.525$. Theoretical predictions.

negligible, while the increase of inclusions up to 40 vol% seems responsible for a severe increase of attenuation up to the highest frequencies tested.

In Fig. 7(b), the theoretical phase velocity curves vs. frequency are depicted. Although the increase of inclusion content seems to have an impact on the dispersion exhibited, this effect is hardly comparable to the experimental dispersion depicted in Fig. 5.

The increase of high-frequency attenuation with sand content, depicted in Fig. 3 is very close to linear. An example is given in Fig. 8. There, the attenuation vs. sand content relationship is depicted for three discrete frequencies of material with $w/c = 0.45$, while the corresponding theoretical predictions are also included. It is suggested that an increase in sand quantity results in approximately proportional increase in attenuation even for as heavy a concentration as 40%. This indicates that multiple scattering mechanisms are weak, since else a deviation from linearity would be manifested, as is the case for a number of aqueous suspensions that exhibit strongly multiple scattering behavior for concentrations lower than 10% (Farrow et al., 1995; Gomez Alvarez-Arenas et al., 2002). The theoretical curves predict this increase exaggerating slightly the attenuation values.

3.2. Air bubble contribution

Besides the relatively weak contribution to measured dispersion, sand particles do not seem adequate to explain the low-frequency attenuation observed as well; see Fig. 3. Therefore, these trends should be attributed to other sources of

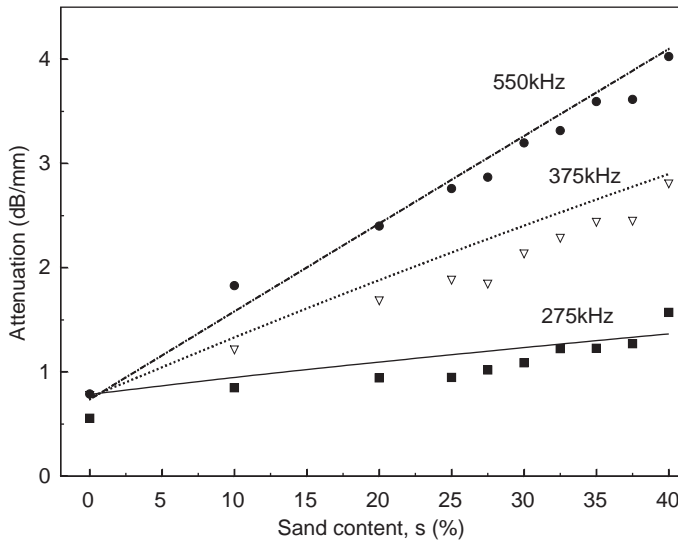


Fig. 8. Effect of sand content on attenuation for different frequencies on mortar with $w/c = 0.45$. Symbols stand for experimental measurements and curves for theoretical predictions.

inhomogeneity. Indeed, no matter how sufficient the compaction may be, there is always an amount of entrapped air bubbles that varies from 1 to even 10 vol% for poor compaction of concrete. Air bubbles in liquid, in concentration even as low as 10^{-4} , have been reported to result in a strong attenuation peak for moderate frequencies and considerable dispersion (phase velocity of even 10000 m/s) up to about the same frequency (Temkin, 2000) while their presence seems to result in low pulse velocity and high attenuation of fresh concrete examined with frequencies in the audible range (Arnaud and Thinet, 2003). Their presence is generally expected to influence to a great extent the wave propagation behavior of cementitious materials due to the so-called “resonant scattering” of the bubbles (Sayers and Dahlin, 1993). Therefore, the problem of scattering on a cavity suspended in a liquid matrix should also be addressed.

Although the continuous matrix medium of mortar is cement paste, with sand particles and air bubbles suspended in it, the present theoretical predictions are made by considering the air bubbles suspended in the effective mortar medium, whose properties are derived in terms of those of both cement paste and sand as depicted in Fig. 6(b). This is evident since, as seen in Fig. 3, although the same cement paste is used ($w/c = 0.525$), the addition of sand grains gradually reduces the low-frequency (<300 kHz) attenuation. Such a behavior originates more likely from the reinforcement of the surrounding medium due to the stiff sand particles. This can be readily understood considering the difference between easily flowable paste and the much less flowable mortar containing a great amount of sand. Indeed, attenuation theoretical results show that although air bubbles are responsible for a large amount of attenuation when suspended in a liquid matrix, they do not exhibit

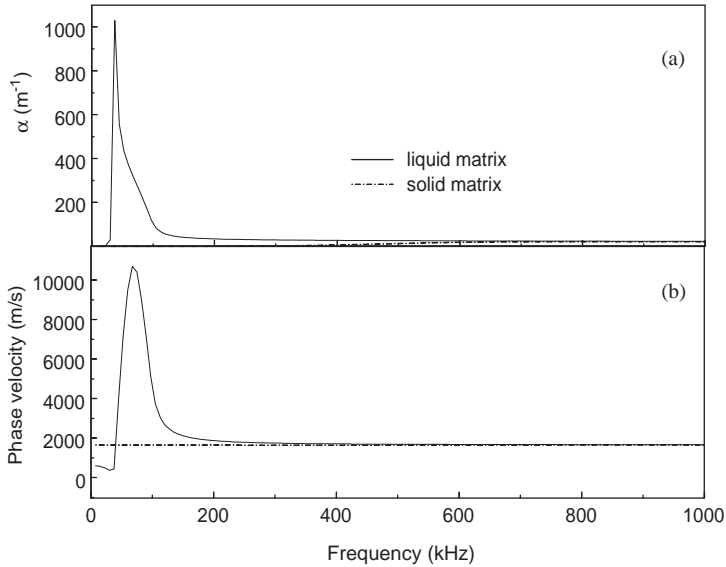


Fig. 9. Effect of matrix shear rigidity on theoretical attenuation coefficient (a) and phase velocity (b) vs. frequency curves for a medium containing 1 vol% of 1 mm air bubbles.

similar behavior when surrounded by an elastic matrix. This is demonstrated in Fig. 9(a) where the attenuation coefficient α vs. frequency curve of a 1 vol% of 1 mm air bubbles in water suspension ($\mu = 100$ Pa) is compared to that of a porous (1 vol%.) elastic material with $\mu = 1.5$ GPa. Fig. 9(b) depicts the corresponding dispersion. It is clear that bubbles, even in small percentage, suspended in liquid matrix (low μ) strongly influence wave propagation, while they cause negligible effects when surrounded by a solid matrix.

The problem of scattering from the entrapped air bubbles in mortar is solved according to the Ying and Truell (1956) formulation considering scattering on a spherical cavity. Therefore, before being introduced in the scattering model, the physical properties should be modified according to the composition of mortar, i.e. the w/c ratio and sand content, in order to yield reasonable predictions. The density of mortar is again calculated from Eq. (6), and the effective bulk modulus from Eq. (7). The value of shear rigidity, μ , is a very important parameter concerning bubble behavior, as it influences crucially dispersion and attenuation, as seen in Fig. 9. Fresh concrete or mortar is a special case of material exhibiting no clear characteristics of either liquid or solid medium, making the use of well-established models for effective shear properties of suspensions of solid particles in solids (Cristensen, 1990) or particles in viscous liquid (Cristensen, 1979) troublesome.

Therefore, the value of shear modulus, μ , was adjusted after comparison of theoretical predictions with “guide” attenuation curves obtained experimentally. As a guide, examples from the experimental database were used and specifically the

curves of Fig. 3(a) are such cases. There, the effect of sand content on the attenuation vs. frequency curve for $w/c = 0.50$ material is depicted. As it has been mentioned in the above, it is obvious that the increase of inclusion content has a dramatic positive impact on high-frequency attenuation, and a negative impact on the low-frequency one. It is worth noting that for a certain low-frequency range, the attenuation of sand rich mortar is negative, meaning that the amplitude was even greater than the amplitude of the water specimen at the same range. In Fig. 10, the attenuation vs. frequency curves theoretically obtained using multiple scattering theory for the bubble case are presented. Air bubble size distribution data applied in the model are given in Table 1. Using density and bulk modulus from Eqs. (6) and (7), the value of μ was adjusted so that the theoretical curve matches the experimental data for each case of different s . The shear modulus used is generally in linear correlation with the density obtained from Eq. (6). Specifically for the cases of paste ($s = 0\%$), and mortar with $s = 27.5\%$, $s = 37.5\%$ and $s = 40\%$, the applied values for μ were, respectively, 60, 262, 376 and 500 MPa, leading to the following relation between μ and ρ_m :

$$\mu = 1.3185 \times 10^6 \rho_m - 2.367 \times 10^9, \quad (9)$$

where ρ_m is in kg/m^3 and μ in Pa.

Therefore, using the above procedure based on a small number of guiding experimental curves, the value of all physical properties of interest to be used in the model can be obtained by simply knowing w/c and sand content through Eqs. (6), (7) and (9) for any particular mixture. Then the scattering coefficients obtained by the Ying and Truell formulation are used to calculate the forward and backward scattering amplitudes through Eq. (2). Using the Waterman and Truell dispersion

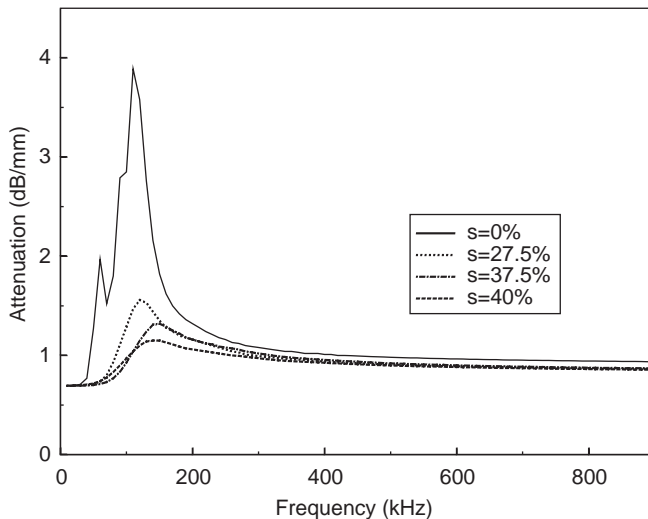


Fig. 10. Effect of sand content on frequency-dependent attenuation of mortar with $w/c = 0.525$. Theoretical predictions.

relation as modified in McClements (2000) that accounts for different populations of scatterers, Eq. (5), the effective wavenumber is obtained, and through Eq. (4), predictions concerning phase velocity and attenuation of the suspension of bubbles in mortar are derived.

It is noted that increase of the experimental database could result in a different and perhaps more precise relationship between the effective shear modulus and composition parameters as the w/c and sand content. The significance, however, of the present approach lies in the dependence of mortar shear rigidity on the composition, which through density is expressed in a simple though adequate manner.

4. Comparison between theoretically predicted and experimental attenuation

4.1. Sand content effect

Solving independently the two aforementioned problems, theoretical predictions concerning the attenuation in mortar are very close to the experimental results. Typical cases are shown in Fig. 11. There, experimentally measured attenuation vs. frequency curves for $w/c = 0.50$ mortar for various sand contents is depicted (Fig. 11(a)). The corresponding theoretical predictions are displayed in Fig. 11(b). Attenuation in region I is dominated by bubble behavior, while region II is characterized by the sand scattering contribution. It is obvious that scattering from

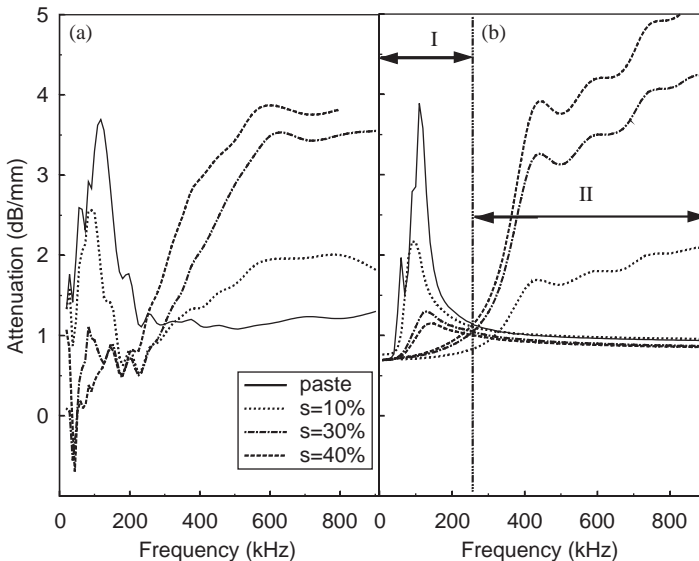


Fig. 11. Comparison of experimental (a) and theoretical (b) attenuation curves of mortar with $w/c = 0.50$; sand content effect.

air bubbles explains the low-frequency attenuation, with the shear rigidity and therefore the bubble behavior being controlled by the sand content. On the other hand, attenuation at high frequencies is exclusively dominated by the scattering on sand particles, the increase of their content leading also to a clear increase of attenuation.

Generally, the effective shear modulus calculated from Eq. (9) results in values around 50 MPa for paste ending about an order of magnitude higher for highly concentrated mortar. Although the value of the shear modulus of the matrix has practically no effect on the sand attenuation (at high frequencies) it controls the low-frequency attenuation in a way matching closely the experimental results. Since no information about the air content of mortar specimens was available, the total volume fraction of air bubbles applied in the theoretical model was constant throughout all cases. However, due to appropriate modification of the effective shear modulus, bubble influence becomes negligible for sand rich mixes, following closely the experimental curves. The assumption that the shear modulus of mortar is lower than the bulk modulus is common for fresh concrete, while only when the hardening develops can it reach the order of magnitude of the bulk modulus (Arnaud and Thinet, 2003). Additionally, in the same work, based on experimentally measured pulse velocity and attenuation coefficient, values between 10^7 and 10^8 Pa have resulted in the effective shear viscoelastic modulus of fresh concrete specimens, which are in agreement with the values used in the present investigation.

The diameter of the sand grain applied to the model is a mean value since the grains used were of size 1–4 mm. Concerning air bubbles, however, not only a single size was assumed. In case a single population of bubbles is assumed to be present, the frequency of the “bubble resonance”, i.e. the frequency f_r where the maximum attenuation is observed, is directly related to the bubble radius, r_{air} , as well as the density of the matrix ρ_m , according to Sayers and Dahlin (1993), Gaunard and Überall (1982) with

$$f_r = \frac{1}{2\pi} \sqrt{\frac{3\rho_{\text{air}}C_{\text{air}}^2}{\rho_m r_{\text{air}}^2}}, \quad (10)$$

where ρ_{air} and C_{air} stand for air density and sound velocity, respectively.

The accidentally entrapped bubble size is generally defined by the size of the aggregates (Neville, 1995), while a random distribution of bubble sizes is generally expected. Since the experimental attenuation at low frequencies presents a broad peak, exhibiting multi-modal behavior, a number of different bubble sizes were assumed in the theoretical investigation. The sizes were adjusted from paste to mortar to the values of Table 1.

4.2. Water content influence

The water content does not seem to be a key factor for attenuation, as experimental curves obtained from specimens with different w/c and the same sand content and size are very close to each other. This is depicted in Fig. 12(a), where

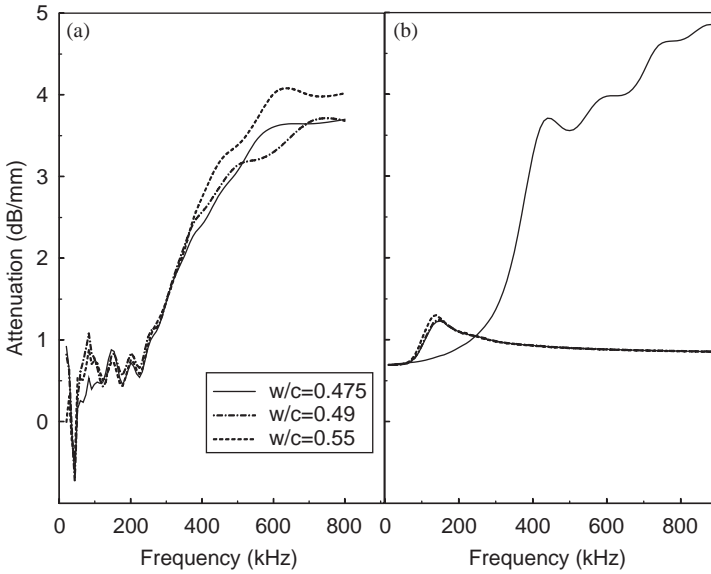


Fig. 12. Comparison of experimental (a) and theoretical (b) attenuation curves of mortar with $s = 35\%$; w/c effect.

curves belong to specimens with $s = 35\%$, while the w/c varies from 0.475 to 0.55. The curves lie one on top of the other, at least in the range up to 350 kHz, and this is predicted by the scattering theory as seen in Fig. 12(b). The different curves were obtained using Eqs. (6), (7) and (9) for the density, bulk and shear modulus of mortar as explained above. Specifically, the density of w/c 0.475 mortar was calculated as 2150 kg/m^3 while that of w/c 0.55 to the value 2100 kg/m^3 , and the shear modulus takes values from 469 to 406 MPa, respectively. It seems that these changes are too small to produce any remarkable discrepancies in the attenuation behavior for the bubble case. It is worth noting that the sand model predicts exactly the same attenuation curve for all 3 cases; thus, only one curve is seen in the respective graph.

4.3. Sand grain size influence

The influence of the sand grain size on attenuation is depicted in Fig. 13(a) and (b) for experiment and for theoretical results, respectively. Using a simple sieve, sand was separated into two fractions with size smaller and larger than 1 mm respectively. The mean size of coarse sand was assumed to be approximately 2.8 mm and of the fine 0.4 mm while modeling the intermediate case, two equal populations of the above sizes were assumed. The w/c ratio of the material is 0.55, while the sand content is 37.5%. It is seen how dramatically the size influences attenuation especially at frequencies above 300 kHz. This is expected since scattering from grains is considered the dominant wave propagation mechanism in these frequencies.

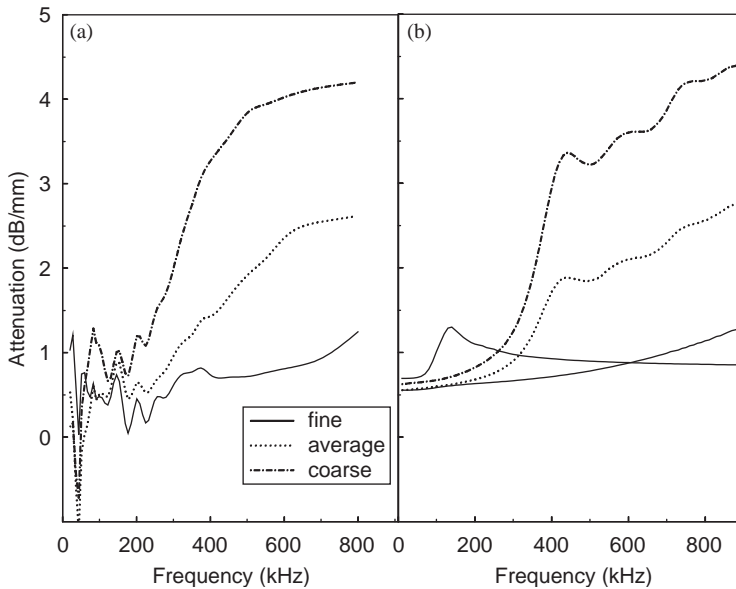


Fig. 13. Effect of sand particle size on experimental (a) and theoretical (b) attenuation curves of mortar with $s = 37.5\%$ and $w/c = 0.55$.

Therefore, although the values of the physical properties, through Eqs. (6), (7), (9) used for all three cases are constant (since the mix design parameters, w/c and $s\%$, remain unchanged) the material does not behave as homogeneous, with the inclusion size being of great importance. Since physical properties are constant, the predictions of the air bubble model are the same for all three cases. It is noted that throughout the rest of the experimental series coarse sand was used to lead to more pronounced effects.

As seen in Fig. 13, the size of the inclusion plays a very important role in attenuation. This is the reason why concerning aggregate scattering, cement paste is considered, in the framework of this analysis, as the homogeneous host medium. The cement grain size generally falls below $50\ \mu\text{m}$ (Neville, 1995). Therefore, it cannot be assumed responsible for the strong scattering action due to the fact that even for the highest frequencies tested, namely 1 MHz, the wavelength λ (approximately 1.5 mm) is about 30 times larger than the cement grain size. In terms of dimensionless frequency ($2\pi r/\lambda$), where r is the scatterer radius, the corresponding values for cement and sand grain are of the order of 0.1 and 10, respectively. It can be seen that increase of ($2\pi r/\lambda$) is accompanied by an increase in attenuation, at least for this order of values (Ye, 1997).

Nevertheless, the theoretical solution of the problem of scattering on a 40 vol% suspension of cement grains of diameter $40\ \mu\text{m}$ in water (corresponding to cement paste with $w/c = 0.50$) yields the attenuation coefficient and phase velocity curves of Fig. 14(a) and (b), respectively. It is seen that the attenuation coefficient is negligible

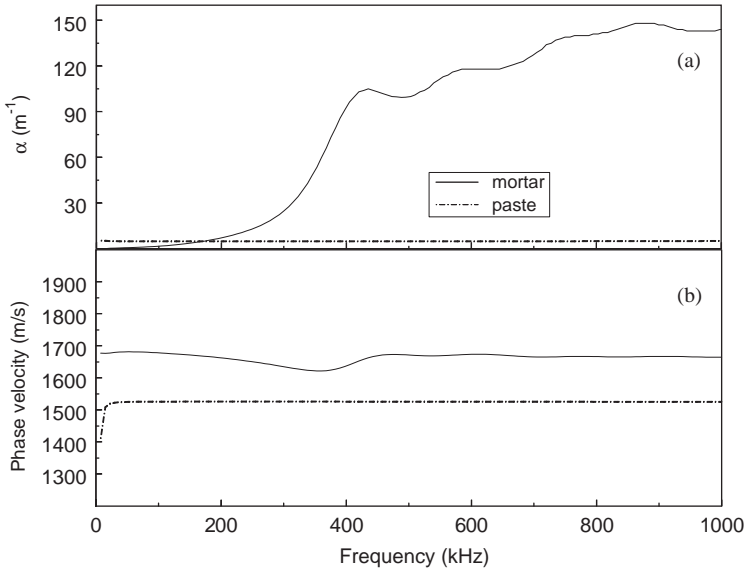


Fig. 14. Attenuation coefficient (a) and phase velocity (b) vs. frequency curves for suspensions of cement grains (40 vol%) in water and sand grains (10 vol%) in cement paste.

compared to that of a 10 vol% of sand grains with diameter 2.8 mm in cement paste at these frequencies which is also seen in Fig. 14(a). Additionally, neither cement nor sand imposes serious dispersion compared to the dispersion when air bubbles are present. Therefore, it is concluded that cement grains are insufficient for strong scattering interference at these frequencies. A certain influence, however, is exercised in the density of mortar and is taken into account, since cement density is around 3150 kg/m^3 , and the water to cement proportion can alter the mortar's density to a certain degree through Eq. (6).

5. Comparison of phase velocity measurements with theoretical predictions

Experimental results concerning velocity dispersion in fresh mortar are presented in Fig. 15. The four cases depicted concern mortar with sand content 30% and w/c that varies from 0.46 to 0.55. The value of phase velocity starts, for most cases, at a value below 1000 m/s for 20 kHz climbing to a maximum between 100 and 150 kHz which is approximately 2300 m/s for $w/c = 0.46$ specimen and almost 4000 m/s for $w/c = 0.55$ mortar. For higher frequencies though, above 300 kHz, no serious discrepancy between the curves is noticed with all different w/c mortars exhibiting phase velocities of approximately 1650 m/s staying constant up to the highest frequency tested. Therefore, from this figure, it seems that the water content has an impact at moderate frequencies, around 150 kHz, where higher water content yields also higher phase velocities. As has been stated in the above, high w/c results in

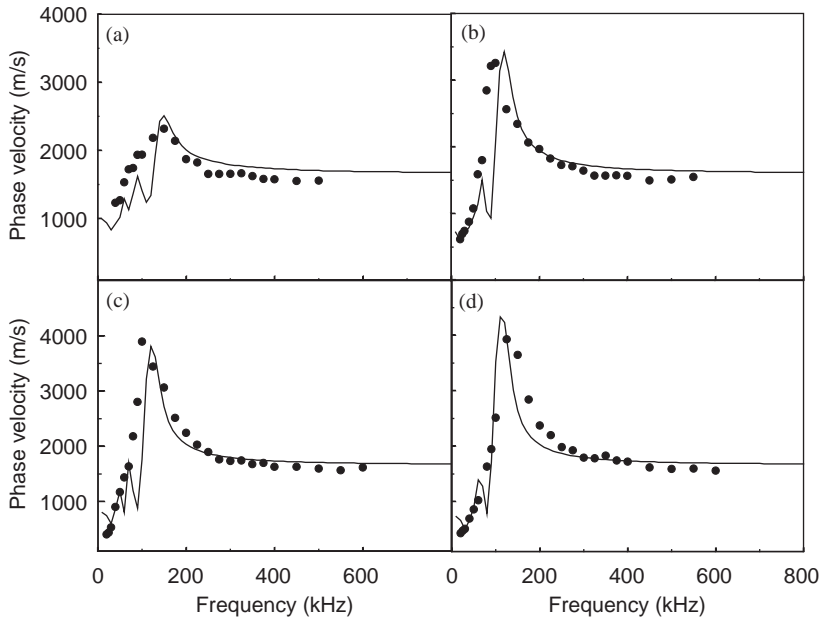


Fig. 15. Phase velocity vs. frequency for mortar with $s = 30\%$ and w/c 0.46 (a), 0.475 (b), 0.525 (c) and 0.55 (d). Symbols stand for experimental measurements and curves for theoretical predictions.

lower density and consequently to the decrease of physical properties of mortar which is the host medium concerning the air bubbles scattering. The increase in water content that is accompanied by the increase of experimental phase velocities around 150 kHz is modeled by the change of density and bulk modulus according to Eqs. (6) and (7) and the decrease of shear modulus, μ , of mortar which specifically obtains the values 50, 30, 25 and 20 MPa for $w/c = 0.46, 0.475, 0.525$ and 0.55. Using these suitable values of μ , i.e. making no use of Eq. (9), the theoretical predictions concerning mortar phase velocity can also be seen in Fig. 15. These curves are obtained from the unique problem of scattering on air bubbles, since as seen in Fig. 7(b), sand scattering causes negligible dispersion compared to bubbles; see Fig. 9(b). Compared to other cases of suspensions, i.e. scattering on an elastic inclusion in liquid matrix, dispersion due to air bubbles is much more significant (Ye, 1997), even at low concentrations due to resonance effects caused by severe density discrepancies between the different phases.

The effect of sand content seems also to be important; see Fig. 16. For all specimens of this figure, w/c equals 0.55 while the sand content varies from 0% (cement paste) to 40%. It follows that the increase of sand content has the opposite effect of adding water. The stiffer the mortar, due to increasing sand amount, the less the dispersion presented, since the maximum phase velocity of paste, at 150 kHz, is above 9000 m/s, while for sand-rich mixes (30% and 40%) and the same frequency, it falls below 4000 m/s. The shear modulus applied in the model is 5, 8.5, 20, 25 MPa

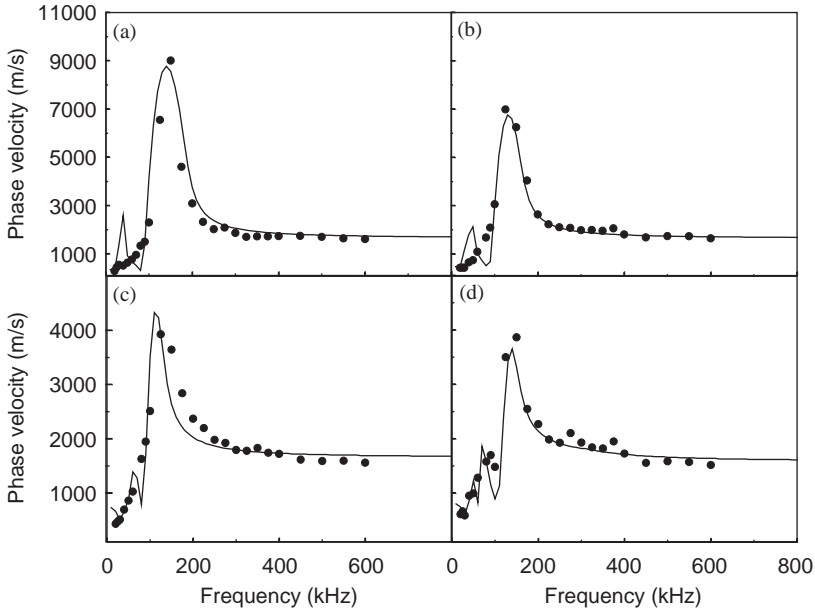


Fig. 16. Phase velocity vs. frequency for mortar with $w/c = 0.55$ and s 0% (a), 25% (b), 30% (c) and 40% (d). Symbols stand for experimental measurements and curves for theoretical predictions.

increasing according to the sand content. Although in the case of phase velocity modeling, the connection between the selected shear modulus and composition is not as straight as it was for the attenuation case, the trend of μ depending on density still holds, with somewhat lower values necessary.

This discrepancy between applied values of shear rigidity to fit experimental attenuation and phase velocity data should receive further consideration. As stated above, attenuation in mortar is very much influenced by the air bubbles, whose resonance behavior is controlled by the shear rigidity of the surrounding medium; e.g. see Fig. 3. It is well known from engineering experience that another parameter crucially affecting resonance peaks is dissipation. Any resonance phenomena are smoothed out in case dissipation mechanisms are considered. In the present case, experimental trends exhibit decrease of low-frequency attenuation with the addition of sand which is more likely the manifestation of the combined effect of increased shear reinforcement due to sand but also increased dissipative behavior due to the visco-inertial mechanisms that originate from the density discrepancy between sand grains and paste. Therefore, since only lossless scattering is considered in the attenuation modeling, it is reasonable that the applied values of shear modulus, μ , to control bubble behavior, are high enough in order to also account for the dissipation that is not included in the model. This is probably the reason why application of the previously developed procedure for defining μ through Eq. (9) for theoretical phase velocity results seems inadequate to fit experimental data due to the small dispersion predicted as the result of air bubbles constrained in a more rigid surrounding

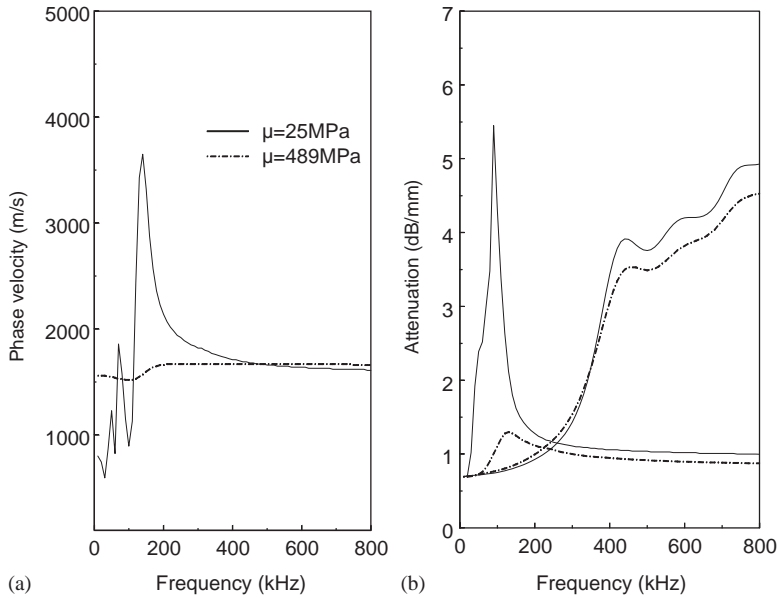


Fig. 17. Effect of mortar shear modulus on theoretical predictions of phase velocity (a) and attenuation (b) for mortar.

medium. Experimental dispersion, instead, exhibits a much more steep velocity change at around the frequency of 150 kHz, a trend that requires for the scattering model the use of shear modulus values of about an order of magnitude lower than calculated through Eq. (9), as seen in Figs. 15 and 16. An example of the above-mentioned discrepancy is provided in Fig. 17(a). There, for the case of mortar with $s = 40\%$, the dispersion predicted using μ through Eq. (9), i.e. 489 MPa, is almost negligible compared to the experimentally measured; see Fig. 16. Efficient modeling of phase velocity requires a much smaller value of μ , namely 25 MPa, as it has also been seen in Fig. 16. Additionally, in Fig. 17(b), an example concerning attenuation modeling of a mortar with $s = 40\%$ is depicted. In this case, efficient modeling requires a value of μ around 500 MPa; see Fig. 7. However, using the shear modulus fit for the modeling of $s = 40\%$ mortar phase velocity (25 MPa), the attenuation curve exhibits a much sharper peak at approximately 100 kHz. Apart from this, it is again seen that beyond bubble resonance frequency region, above 300 kHz, the curves provided using different shear moduli are not much affected.

It is mentioned that in the search for a unified model to describe adequately the behavior of the entire frequency range up to 1 MHz, the dispersion relation expressed by Eq. (3) provides results matching almost exactly the individual curves predicted from the problem of (i) sand scattering in paste and (ii) air bubble in mortar as if they were simply superimposed. The wavenumber k_c was set equal to $2\pi f/1650\text{m}^{-1}$. Although the dispersion relation applies to cases of different

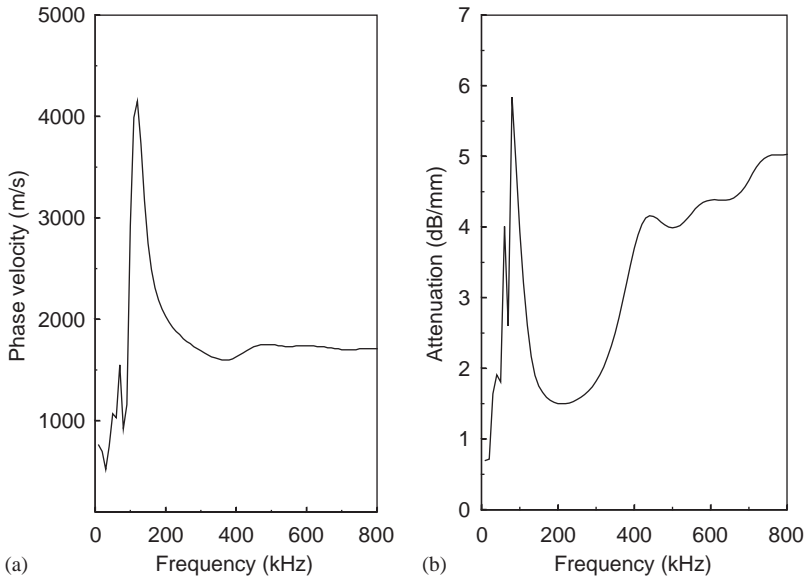


Fig. 18. Phase velocity (a) and attenuation (b) obtained using modified dispersion relation Eq. (5).

populations embedded in the same matrix, it is seen that, more likely due to the small phase velocity discrepancy of void free paste and mortar (see, for example, Figs. 5 and 16 for high frequencies above severe bubble interference) it yields quite reasonable results. This can be seen in Fig. 18(a) where Eq. (3) yields a dispersion curve for the case of material with $\mu = 25$ MPa very close to the one depicted in Fig. 17(a) concerning the unique problem of bubble scattering in mortar, while the attenuation curve (Fig. 18(b)) seems to be like the superposition of the attenuation curves individually produced by the solution of the two problems.

6. Concluding remarks

The aim of the present work is to contribute to the understanding of wave propagation in fresh cementitious material. Since the material at hand is strongly inhomogeneous, extraction of specific and valuable information depends on the correct interpretation of ultrasonic data. The experimental measurements along with predictions from scattering theory, demonstrate the dominant effect of sand grains on high-frequency attenuation. Similarly, the effect of shear reinforcement of the matrix with sand seems to be the answer to the controlled air bubble influence on dispersion and attenuation at low frequencies. In case air content is known, experimental values of phase velocity around 150 kHz could be a good indicator of the w/c ratio values. Indeed, increased dispersion around that frequency range, as shown, could be due to increase of w/c (through a decrease in density and shear

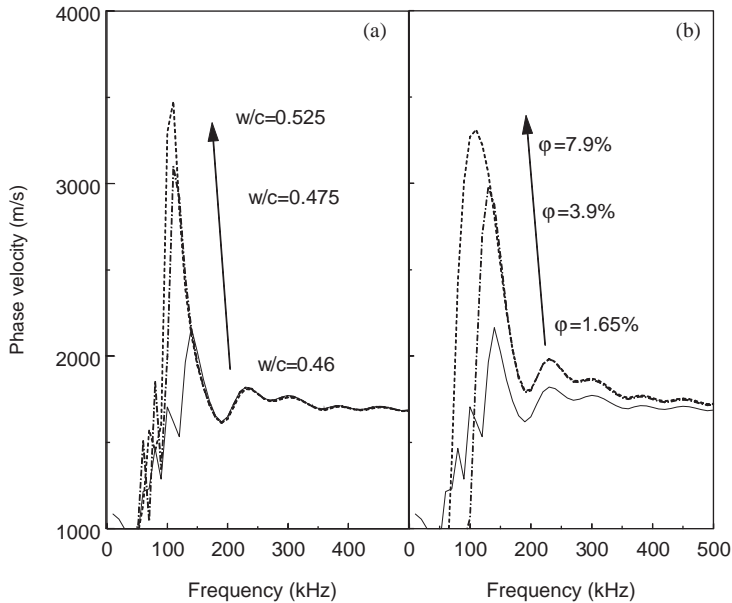


Fig. 19. Effect of w/c on mortar dispersion with constant air content of 1.65% (a) and effect of air content on mortar dispersion with constant $w/c = 0.46$ (b).

modulus), as is seen in the example of Fig. 19(a) with theoretical predictions. However, similar phase velocity increase could be the result of air content increase holding the w/c constant, as seen in Fig. 19(b). Therefore, simultaneous measurement of air content with commercially available devices and application of its value to the scattering model can indicate the w/c value, which interacting with this specific air content is responsible for the measured dispersion. Apart from this, the application of such a technique in fresh concrete would be of even greater importance. This of course demands larger specimen size, due to coarse aggregates present in concrete as well as equipment capable of transmitting signals through several centimeters of heavily attenuative material.

References

- Abrams, D.A., 1918. Design of concrete mixtures. Bulletin No.1, Structural Materials Laboratory, Lewis Institute, Chicago, pp. 1–20.
- Aggelis, D.G., Philippidis, T.P., 2004. Ultrasonic wave dispersion and attenuation in fresh mortar. *NDT&E INT* 37(8), 617–631.
- Akkaya, Y., Voigt, T., Subramaniam, K.V., Shah, S.P., 2003. Nondestructive measurement of concrete strength gain by an ultrasonic wave reflection method. *Mater. Struct.* 36, 507–514.
- Allegra, J.R., Hawley, S.A., 1972. Attenuation of sound in suspensions and emulsions: theory and experiments. *J. Acoust. Soc. Am.* 51 (5), 1545–1564.
- Arnaud, L., Thinet, S., 2003. Mechanical evolution of concrete during setting. *Mater. Struct.* 36, 355–364.

- Bescher, E., Sambol, M., Rice, E.K., Mackenzie, J.D., 2004. Determination of water-to-cement ratio in freshly mixed rapid-setting calcium sulfoaluminate concrete using 2.45 GHz microwave radiation. *Cem. Concrete Res.* 34(5), 807–812.
- Boumiz, A., Vernet, C., Cohen Tenoudji, F., 1996. Mechanical properties of cement pastes and mortars at early ages. *Adv. Cem. Based Mater.* 3, 94–106.
- Boutin, C., Arnaud, L., 1995. Mechanical characterization of heterogeneous materials during setting. *Eur. J. Mech. A/Solids* 14 (4), 633–656.
- Casson, R.B., Domone, P.I.J., 1982. Ultrasonic monitoring of the early age properties of concrete. Proceedings of the International Conference on Concrete at Early Ages, ECNP, Paris, pp. 129–135.
- Challis, R.E., Tebbutt, J.S., Holmes, A.K., 1998. Equivalence between three scattering formulations for ultrasonic propagation in particulate mixtures. *J. Phys. D* 31, 3481–3497.
- Chotard, T., Gimet-Breart, N., Smith, A., Fargeot, D., Bonnet, J.P., Gault, C., 2001. Application of ultrasonic testing to describe the hydration of calcium aluminate cement at the early age. *Cem. Concrete Res.* 31, 405–412.
- Cristensen, R.M., 1979. *Mechanics of Composite Materials*. Wiley, New York.
- Cristensen, R.M., 1990. A critical evaluation for a class of micromechanics models. *J. Mech. Phys. Solids* 38 (3), 379–404.
- D'Angelo, R., Plona, T.J., Schwartz, L.M., Coveney, P., 1995. Ultrasonic measurements on hydrating cement slurries. *Adv. Cem. Based Mater.* 2, 8–14.
- Dukhin, A.S., Goetz, P.J., 1996. Acoustic spectroscopy for concentrated polydisperse colloids with low density contrast. *Langmuir* 12, 4998–5003.
- Epstein, P.S., Carhart, R.R., 1953. The absorption of sound in suspensions and emulsions. I. Water for in air. *J. Acoust. Soc. Am.* 25 (3), 553–565.
- Farrow, C.A., Anson, L.W., Chivers, R.C., 1995. Multiple scattering of ultrasound in suspensions. *Acustica* 81, 402–411.
- Garnier, V., Corneloup, G., Sprauel, J.M., Perfumo, J.C., 1995. Setting time study of roller compacted concrete by spectral analysis of transmitted ultrasonic signals. *NDT&E INT* 28 (1), 15–22.
- Gaunard, G.C., Überall, H., 1982. Resonance theory of the effective properties of perforated solids. *J. Acoust. Soc. Am.* 71 (2), 282–295.
- Gomez Alvarez-Arenas, T.E., Elvira Segura, L., Riera Franco de Sarabia, E., 2002. Characterization of suspensions of particles in water by an ultrasonic resonant cell. *Ultrasonics* 39, 715–727.
- Grosse, C.U., Reinhardt, H.W., 1994. Continuous ultrasound measurement during setting and hardening of concrete. *Otto Graf J.* 5, 76–98.
- Grosse, C.U., Reinhardt, H.W., 2001. Fresh concrete monitored by ultrasound methods. *Otto Graf J.* 12, 157–168.
- Head, W.J., Phillipi, H.M., Howdyshell, P.A., Lawrence, D., 1983. Evaluation of selected procedures for the rapid analysis of fresh concrete. *Cem. Concrete Aggregates CCAGDP* 5 (2), 88–102.
- Herb, A.T., Grosse, C.U., Reinhardt, H.W., 1999. Ultrasonic testing device for mortar. *Otto Graf J.* 10, 144–155.
- Hipp, A.K., Storti, G., Morbidelli, M., 1999. On multiple-particle effects in the acoustic characterization of colloidal dispersions. *J. Phys. D* 32, 568–576.
- Holmes, A.K., Challis, R.E., Wedlock, D.J., 1993. A wide bandwidth study of ultrasound velocity and attenuation in suspensions: comparison of theory with experimental measurements. *J. Colloid Interface Sci.* 156, 261–268.
- Keating, J., Hannant, D.J., Hibbert, A.P., 1989. Correlation between cube strength, ultrasonic pulse velocity and volume change for oil well cement slurries. *Cem. Concrete Res.* 19 (5), 715–726.
- Kinra, V.K., Petratis, M.S., Datta, S.K., 1980. Ultrasonic wave propagation in a random particulate composite. *Int. J. Solids Struct.* 16, 301–312.
- Labouret, S., Looten-Baquet, I., Bruneel, C., Frohly, J., 1998. Ultrasound method for monitoring rheology properties evolution of cement. *Ultrasonics* 36, 205–208.
- Malhotra, V.M., Carino N.J., (Eds.), 1991. *CRC Handbook on Nondestructive Testing of Concrete*. CRC Press, Boca Raton, FL.
- Mather, B., 1976. How soon is soon enough? *ACI J.* 73 (3), 147–150.

- McClements, D.J., 2000. Ultrasonic measurements in particle size analysis. In: Meyers, R.A. (Ed.), *Encyclopedia of Analytical Chemistry*. Wiley, Chichester.
- Mubarak, K., Bois, K.J., Zoughi, R., 2001. A simple, robust, and on-site microwave technique for determining water-to-cement ratio (w/c) of fresh Portland cement-based materials. *IEEE Trans. Instrum. Meas.* 50 (5), 1255–1263.
- Neville, A.M., 1995. *Properties of Concrete*. Longman, London.
- Ozturk, T., Rapoport, J., Popovics, J.S., Shah, S.P., 1999. Monitoring the setting and hardening of cement-based materials with ultrasound. *Concrete Sci. Eng.* 1, 83–91.
- Pao, Y.H., Mow, C.C., 1963. Scattering of plane compressional waves by a spherical obstacle. *J. Appl. Phys.* 34 (3), 493–499.
- Popovics, S., Popovics, J.S., 1998. Ultrasonic testing to determine water–cement ratio for freshly mixed concrete. *Cem. Concrete Aggr.* 20 (2), 262–268.
- Rapoport, J.R., Popovics, J.S., Kolluru, S.V., Shah, S.P., 2000. Using ultrasound to monitor stiffening process of concrete with admixtures. *ACI Mater. J.* 97 (6), 675–683.
- Reinhardt, H.V., Grosse, C.U., Herb, A.T., 2000. Ultrasonic monitoring of setting and hardening of cement mortar—a new device. *Mater. Struct.* 33, 580–583.
- Sayers, C.M., Dahlin, A., 1993. Propagation of ultrasound through hydrating cement pastes at early times. *Adv. Cem. Based Mater.* 1, 12–21.
- Subramanian, V.K., Rapoport, J.R., Shah, S.P., 2000. Nondestructive technique for monitoring strength gain in concrete structures. *Cementing Future* 12 (1), 4–5.
- Temkin, S., 2000. Attenuation and dispersion of sound in dilute suspensions of spherical particles. *J. Acoust. Soc. Am.* 108 (1), 126–146.
- Valic, M.I., 2000. Hydration of cementitious materials by pulse echo USWR Method, apparatus and application examples. *Cem. Concrete Res.* 30, 1633–1640.
- Waterman, P.C., Truell, R., 1961. Multiple scattering of waves. *J. Math. Phys.* 2, 512–537.
- Ye, Z., 1997. Acoustic dispersion and attenuation in many spherical scatterer systems and the Kramers–Kronig relations. *J. Acoust. Soc. Am.* 101 (6), 3299–3305.
- Ye, G., vanBreugel, K., Fraij, A.L.A., 2003. Experimental study and numerical simulation on the formation of microstructure in cementitious materials at early age. *Cem. Concrete Res.* 33, 233–239.
- Ying, C.F., Truell, R., 1956. Scattering of a plane longitudinal wave by a spherical obstacle in an isotropically elastic solid. *J. Appl. Phys.* 27 (9), 1086–1097.